To be published in Photonics Research:

Title: Single-shot optical transfer delay measurement with sub-picosecond accuracy and sub-millisecond range

Authors: Lihan Wang,Xiangchuan Wang,Xi Liu,Yue Yang,Shupeng Li,Sihao Yang,Qianwen Sang,Zhijian Zhang,Jingxian Wang,Shilong Pan

Accepted: 28 February 25

Posted 03 March 25

DOI: https://doi.org/10.1364/PRJ.536776

Single-shot optical transfer delay measurement with sub-picosecond accuracy and sub-millisecond range

Lihan Wang,[1] Xiangchuan Wang,[1,*] Xi Liu,[1] Yue Yang,[1] Shupeng Li,[2] Sihao Yang,[1] Qianwen Sang,[1] Zhijian Zhang,[1] Jingxian Wang,[1] and Shilong Pan[1,**]

[1] *National Key Laboratory of Microwave Photonics, Nanjing University of Aeronautics and Astronautics, Nanjing 210016, China*

[2] *Suzhou LiuYaoSi Information Technologies Company, Ltd., Suzhou 215558, China*

[*] *wangxch@nuaa.edu.cn*

[**] *pans@nuaa.edu.cn*

Abstract: Optical transfer delay (OTD) is essential for distributed coherent systems, optically controlled phased arrays, fiber sensing systems, and quantum communication systems. However, existing OTD measurement techniques typically involve trade-offs between accuracy, range, and speed, limiting the application in the fields. Herein, we propose a single-shot OTD measurement approach that simultaneously achieves high-accuracy, long-range, and high-speed measurement. A microwave photonic phase-derived ranging with a nonlinear interval microwave frequency comb (MFC) and a discrete frequency sampling technique is proposed to conserve both frequency and time resources, ensuring high-accuracy and ambiguity-free measurements. In the proof-of-concept experiment, a delay measurement uncertainty at the 10^{-9} level with a single 10 µs sampling time is first reported, to our knowledge. The method is also applied to coherently combine two distributed signals at 31.8 GHz, separated by a 2-km optical fiber. A minimal gain loss of less than 0.0038 dB compared to the theoretical value was achieved, corresponding to an OTD synchronization accuracy of 0.3 ps.

1. Introduction

Optical transfer delay (OTD) is a fundamental and essential parameter in various optical and microwave systems [1–3]. For example, in quantum photonics, an accurate and adjustable OTD is indispensable for large-scale active time multiplexing to improve the generation efficiency of coincident photons [4]. In microwave photonics, phased arrays based on high-precision optical true-time delay lines can better suppress the beam-squint effect for large-bandwidth signals [5, 6]. Moreover, OTD control accuracy directly affects the performance of systems such as distributed coherent aperture radars (DCAR) [7], synthesizing reconfigurable radio-frequency arbitrary waveforms [8], and fiber-based wireless communication systems [9]. However, measuring and adjusting the OTD in feedback-controlled systems can limit loop bandwidth and response speed. In applications involving moving optical links, such as free-space optical communication, the requirement for a measurement refresh rate is significantly high [10]. For example, when the relative movement speed reaches several meters per second, maintaining reliable synchronization requires high-accuracy OTD measurement speeds as high as the kilohertz level.

In the past, the performance of delay measurement techniques was investigated within the context of stationary channels. The delay can be extracted in a cross-correlation process, and research findings, as documented in [11, 12], demonstrate that a probe signal characterized by a two-tone form achieves the lowest Cramér-Rao lower bound (CRLB) on delay measurement. Achieving the CRLB requires a high coherence in the probe signal, which is difficult to achieve in OTD measurement. On the other hand, considering that the optical frequency is easy to drift, traditional methods, including optical time-domain reflectometry (OTDR) [13, 14] and optical frequency-domain reflectometry (OFDR) [15–17] have to apply a broadband probe signal. OTDR-based methods detect the time difference of a probe pulse between the transmission and reception to obtain the OTD. However, the accuracy of these methods is typically low (usually in the nanosecond range) because of the relatively broad width of the probe pulses. Although increasing the number of averages can effectively suppress random errors and noise to improve accuracy, it comes at the cost of a low measurement speed. OFDR-based methods sweep the laser wavelength to realize absolute OTD measurement, in which the measurement accuracy is traced to the stability of the wavelength [16] and the coherence of the optical source [17]. However, wavelength sweeping complicates the measurement system, while broadband spectrum analysis is time-consuming. Furthermore, the measurement accuracy degrades sharply with an increase in OTD. Other technologies based on optical resonators and phase-locked loops have also been proposed for OTD measurement to achieve large-range and high accuracy simultaneously [18, 19]. These methods require strict environmental stability and a large amount of time for measurement. To meet the increasing comprehensive requirements of OTD measurement, some studies have focused on optimizing the OTD measurement speed while ensuring high accuracy and long range. For example, optical frequency combs (OFC) [20–24] show high potential for measuring OTD because they have been widely applied in ranging and can achieve high-speed and accurate distance measurement. However, OFC covering a wide frequency range suffers from severe dispersion and nonlinearity in long optical waveguides such as optical fiber. Moreover, to extend the measurement range, OFC-based methods typically utilize the Vernier effect. This necessitates the use of multiple locked combs, each with a distinct repetition frequency [25]. Consequently, it is imperative not only to ensure that the repetition frequencies with each comb are locked but also to maintain a relatively stable frequency drift among the combs, thereby adding complexity to the architecture of the measurement system.

Phase-derived ranging is resistant to dispersion and the measurement accuracy is not limited by the coherence of the laser [26]. Therefore, it is a promising technology for achieving CRLB for OTD measurement. We reported a phase-derived ranging technology for OTD measurement where the OTD is proportional to the microwave's phase, achieving a measurement accuracy of ±0.04 ps and a measurement speed of 21 Hz [26]. In this method, as the phase detector has a limited range from $-\pi$ to π, a phase unwrapping algorithm is required to resolve the absolute OTD. Therefore, the measurement speed is limited by the switching rate of the microwave signal and the integral time of phase detector. To circumvent the need for switching the microwave signal, some researchers combined phase-derived ranging with other ambiguity-free OTD measurement technologies to enable fast OTD measurement [27–29]. The measurement speed reached the kilohertz range. However, increasing the measurement speed can lead to a reduced signal-to-noise ratio (SNR), potentially causing phase unwrapping failure. This intrinsic limitation associated with high-speed OTD measurement remains to be addressed.

To achieve high-speed and high-accuracy measurement, three critical factors must be considered. First, the limited duration of the probe signal inherently restricts the measurement SNR. Second, high-speed measurements can lead to range ambiguity, where a probe signal might be received after transmitting the subsequent probe signal. Third, the substantial volume of data introduced by the measurement system necessitates a reduction in computational demands for real-time measurement.

This article proposes and demonstrates a microwave photonic phase-derived OTD measurement method based on a nonlinear interval microwave frequency comb (MFC). The proposed method effectively addresses key challenges in high-speed OTD measurement. From a measurement perspective, we makes three key contributions: achieving high-accuracy measurement in high-speed scenarios, enabling ambiguity-free measurements for large-range capabilities, and reducing computational overhead to create a cost-effective and simple system structure. The proposed method employs a phase-derived ranging approach, which overcomes the bandwidth constraint of traditional methods for measurement signals. Therefore, the use of MFC signal enables the measurement accuracy to approach the CRLB under high-speed conditions. To achieve ambiguity-free measurements, we introduce a discrete frequency sampling technique and a novel phase unwrapping method, which reduces the intermediate frequency (IF) filter bandwidth requirements for the receiver. Additionally, for high-speed measurements, our approach requires phase detection of only four known frequencies, providing a computational complexity advantage by lowering the digital matched filtering overhead. Our proposed method demonstrate a delay measurement uncertainty at the 10^{-9} level with a single 10 µs sampling time, offering a practical and efficient solution for rapid OTD measurement in various optical and microwave systems.

2. Principle

2.1. Principle of the single-shot OTD measurement

Several coherent radio-frequency (RF) signals with different frequencies are combined to form an MFC. The MFC is then modulated on the optical carrier as the probe signal, which transmits through the device under test (DUT) and carries the phase information of the OTD. Upon transmission, the received optical signal is transformed into a photocurrent via optical-to-electrical conversion. Mathematically, if we solely consider the corresponding RF components of the MFC, the photocurrent can be expressed as:

$$i(t) = \eta\alpha^2 E_o^2 \sum_{m=1}^{n} \cos\{2\pi f_m(t-\tau)\}, \tag{1}$$

where η is the efficiency of the electronic-to-optical conversion and optical-to-electrical conversion, α is the power loss of the transmission link, E_o is the amplitude of the optical signal, n is the number of the RF signals, f_m is the frequency of the m^{th} RF signal, τ is the OTD under test.

After the optical-to-electrical conversion, the photocurrent is demodulated into multiple single-frequency microwave signals, referred to as frequency points. It is crucial to reserve sufficient frequency intervals to prevent frequency overlap during phase detection. A detailed discussion on the selection of frequency interval is presented in the following section.

From Eq. (1), the OTD can be calculated via the phase variation of the corresponding RF signal. However, the measured phase difference of the RF signal with frequency f_m has an ambiguous value owing to the limited range between $-\pi$ and π of the phase detector and can be expressed as:

$$\begin{aligned} \varphi(f_m) &= 2\pi \cdot N(f_m) - 2\pi f_m \tau \\ &= 2\pi \cdot \left\lfloor \frac{1}{2} + f_m\tau \right\rfloor - 2\pi f_m \tau, \end{aligned} \tag{2}$$

where $N(f_m)$ is an unknown non-negative integer, representing the integer ambiguity of the frequency interval f_m; $\lfloor \ldots \rfloor$ is the rounding operator. Here, $\varphi(f_m)$ can also be considered as the cross-power spectrum's phase term. After the phase unwrapping algorithm, the OTD can be calculated using the following formula:

$$\tau = \frac{-\varphi(f_1) + 2\pi \cdot N(f_1)}{2\pi f_1}. \tag{3}$$

The unknown parameter $N(f_1)$ in Eq. (3) can be calculated by analyzing the phases of the other frequency components in the MFC. The core challenge in MFC-based OTD measurement is resolving the integer ambiguity accurately. With the limited measurement time in high-speed scenarios, it is crucial to carefully select the frequency points. The following section details the discrete frequency sampling method used for rapid phase unwrapping.

2.2. Phase unwrapping algorithm based on discrete frequency sampling

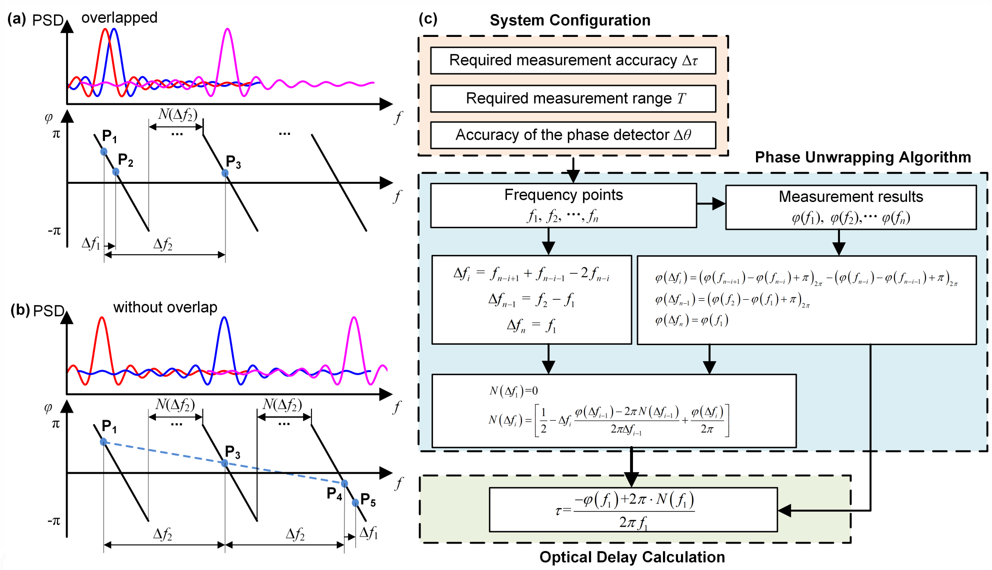

Fig. 1. Illustration of the principle of the proposed phase unwrapping algorithm. (a) Traditional phase unwrapping algorithm based on group delay estimation. (b) The proposed phase unwrapping algorithm based on discrete frequency sampling. PSD, power spectral density. P_1, P_2, and P_3 are the frequency points chosen by the traditional phase unwrapping algorithm. P_1, P_3, and P_5 are the frequency points selected by the proposed phase unwrapping algorithm. P_4 is obtained by linear fitting P_1 and P_3. (c) Flowchart of the proposed OTD measurement process.

To calculate the integer ambiguity, we should first obtain a rough slope of the phase-frequency spectrum. Traditional phase-unwrapping algorithms [26] start by determining the DUT's rough group delay response at a specific frequency. The integer ambiguity is then resolved by linear fitting the phase-frequency curve. In this analysis, we consider three frequency points on the phase-frequency curve labeled P_1, P_2, and P_3, with frequency intervals of Δf_1 and Δf_2, as shown in Fig. 1(a). To accurately determine the group delay around frequency point P_1, the minimum frequency interval Δf_1 must be set smaller than the interval at which the phase exceeds 2π, that is, $|\varphi(f + \Delta f_1) - \varphi(f)| \leq \pi$. By substituting this condition into Eq. (2), the minimum frequency interval should satisfy $\Delta f_1 \leq 1/(2\tau)$. For a DUT longer than 500 µs (approximately 100 km length of fiber), the minimum frequency interval Δf_1 should be smaller than 1 kHz. The acquisition time of the phase detector must be sufficiently long to address the frequency overlap problem and simultaneously extract the phase of each MFC frequency component. According to the Fourier Uncertainty Principle [30], the resolution cannot be infinitely small in both the time and frequency domains. For instance, in a Fourier Transform, the sampling time must exceed 1 ms to distinguish two frequency components with a 1 kHz interval, thereby limiting the minimum sampling time length in the OTD measurement. This can also be interpreted in the time domain: the repetition cycle of the probe signal must be shorter than the measurement range to avoid confusion with the next transmitted probe signal.

A novel phase unwrapping algorithm based on discrete frequency sampling is proposed to reduce the required minimum frequency interval Δf_1 and solve the frequency overlap problem. Fig. 1(b) illustrates the principle of the proposed algorithm. To simplify the analysis, only three frequency points (P_1, P_3, and P_5) in the MFC are considered. The corresponding frequency differences are Δf_2 ($P_1 \rightarrow P_3$), $\Delta f_2 + \Delta f_1$ ($P_3 \rightarrow P_5$), and $2\Delta f_2 + \Delta f_1$ ($P_1 \rightarrow P_5$), respectively. To demonstrate the generality of the algorithm, we assume $N(\Delta f_1)$ is a known non-negative integer. The phase unwrapping algorithm aims to solve the integer ambiguity $N(\Delta f_2)$. The integer ambiguity between frequency points of P_1 and P_3 has a specific relationship with the frequency points P_3 and P_5, which are denoted by $N(\Delta f_2)$ and $N(\Delta f_2) + N(\Delta f_1)$, respectively. The first step is to obtain the phase of frequency point P_4 by linearly fitting P_1 and P_3. The phase difference with a frequency interval of Δf_1 and Δf_2 can then be obtained as follows:

$$\begin{aligned}\varphi(\Delta f_1) &= \Big(\varphi(f_{P5}) - \varphi(f_{P4}) + \pi\Big)_{2\pi} - \pi \\ &= \Big(\varphi(f_{P5}) - \varphi(f_{P3}) + \pi\Big)_{2\pi} - \Big(\varphi(f_{P3}) - \varphi(f_{P1}) + \pi\Big)_{2\pi},\end{aligned} \tag{4}$$

$$\varphi(\Delta f_2) = \Big(\varphi(f_{P3}) - \varphi(f_{P1}) + \pi\Big)_{2\pi} - \pi, \tag{5}$$

where the symbol $(x)_y$ in this paper represents the remainder operator to obtain the remainder from the division of x by y; f_{P1}, f_{P3}, and f_{P5} are the frequencies of points P_1, P_3, and P_5. The modulo operators in Eq. (4) and Eq. (5) are the preprocessing processes used to confine the phase difference in the range from $-\pi$ to π. The integer ambiguity $N(\Delta f_2)$ can then be calculated using the following equation:

$$\begin{aligned}N(\Delta f_2) &= \left\lfloor \frac{1}{2} + \Delta f_2 \cdot \tau + \frac{\varphi(\Delta f_2)}{2\pi} \right\rfloor \\ &= \left\lfloor \frac{1}{2} - \Delta f_2 \frac{\varphi(\Delta f_1) - 2\pi N(\Delta f_1)}{2\pi\Delta f_1} + \frac{\varphi(\Delta f_2)}{2\pi} \right\rfloor.\end{aligned} \tag{6}$$

To verify the phase unwrapping algorithm, we assume that the accuracy of the phase detector is $\Delta\theta$. The detected phase can be expressed as $\varphi(f) = \theta(f) \pm \Delta\theta$, where $\theta(f)$ is the accurate phase of the RF signal. Then, Eq. (6) can be written as:

$$N'(\Delta f_2) = \left\lfloor \frac{1}{2} - \Delta f_2 \frac{\theta(\Delta f_1) - 2\pi N(\Delta f_1)}{2\pi\Delta f_1} + \frac{\theta(\Delta f_2)}{2\pi} \pm (\frac{\Delta f_2}{\Delta f_1} + 1)\frac{\Delta\theta}{\pi} \right\rfloor, \tag{7}$$

where N' represents the calculated integer ambiguity, which should equal the actual integer ambiguity. Noticed that $\theta(\Delta f_2) = 2\pi N(\Delta f_2) - 2\pi\tau\Delta f_2$ and $\theta(\Delta f_1) = 2\pi N(\Delta f_1) - 2\pi\tau\Delta f_1$ are valid, the calculated integer ambiguity can be expressed as:

$$N'(\Delta f_2) = \left\lfloor \overbrace{N(\Delta f_2)}^{\text{Integer}} + \overbrace{\frac{1}{2} \pm \left(\frac{\Delta f_2}{\Delta f_1} + 1\right)\frac{\Delta\theta}{\pi}}^{\text{Error}} \right\rfloor. \tag{8}$$

To make $N'(\Delta f_2) = N(\Delta f_2)$, the choice of the frequency interval Δf_1 and Δf_2 should satisfy the following equation to eliminate the error item in Eq. (8):

$$\Delta f_2 \leq \left(\frac{\pi}{2\Delta\theta} - 1\right)\Delta f_1 \leq \left(\frac{\pi}{2\Delta\theta} - 1\right)\frac{1}{2\tau}. \tag{9}$$

Theoretically, the minimum frequency interval can be increased by $(\pi/2\Delta\theta - 1)$ times compared to traditional phase unwrapping algorithms. When the measurement system processes the IF signal in the analog domain, the proposed discrete frequency sampling method reduces the bandwidth requirement for the filter. In the case of digital signal processing for IF signals, a larger frequency interval allows for frequency domain signal processing with lower resolution. Consequently, the sampling time length can be reduced by the same factor in the proposed OTD measurement system. For instance, if a phase detector has an accuracy of 0.1 deg, the theoretical magnification factor for $\Delta f_2/\Delta f_1$ is 899.

By combining the proposed phase unwrapping algorithm with discrete frequency sampling, we can finally realize a single-shot OTD measurement. For a given measurement range T, the frequency interval should satisfy $\Delta f_1 \leq 1/(2T)$. Based on the selected frequency points and the proposed phase unwrapping algorithm, we can obtain the integer ambiguity $N(\Delta f_2)$ in theory, where $\Delta f_2 < (\pi/2\Delta\theta - 1)\Delta f_1$. If $\Delta f_2 \geq f_1$, we can directly let $\Delta f_2 = f_1$ and solve Eq. (3) to calculate the OTD. Otherwise, when $\Delta f_2 < f_1$, it requires dividing the phase unwrapping process into $(n-1)$ times until $\Delta f_n \geq f_1$. The choice of n frequency points requires the following:

$$\frac{\Delta f_{k+1}}{\Delta f_k} < \frac{\pi}{2\Delta\theta} - 1, k = 1, 2, \cdots, n-1. \tag{10}$$

2.3. Choice of the number of frequency points

In the above subsection, we discuss the constraints on the frequency interval for single-shot and unambiguous measurement. In this section, we provide a brief explanation of how to select the appropriate number of frequency points for measurement. For practical measurements, we first need to confirm the required measurement range T, measurement accuracy $\Delta\tau$, and the accuracy of the phase detector $\Delta\theta$. Based on the equation $\tau = -\theta/2\pi f$, we can calculate the initial frequency $f_1 = \Delta\theta/2\pi\Delta\tau$ used for phase-derived ranging. From Eq. (10), we can further derive the following inequality:

$$\Delta f_n < \Delta f_{n-1}\left(\frac{\pi}{2\Delta\theta} - 1\right) < \ldots < \Delta f_1\left(\frac{\pi}{2\Delta\theta} - 1\right)^{n-1}. \tag{11}$$

We can then derive the relationship between the number of frequency points and the required phase accuracy:

$$\Delta\theta < \frac{\pi}{2\left[\left(\frac{\Delta f_n}{\Delta f_1}\right)^{\frac{1}{n-1}} + 1\right]} \leq \frac{\pi}{2\left[(2f_1 \cdot T)^{\frac{1}{n-1}} + 1\right]}. \tag{12}$$

Fig. 2(a) illustrates this relationship under typical conditions. It shows that increasing the number of MFC frequencies reduces the required phase accuracy, which in turn lowers the SNR requirement for unambiguous measurement. Increasing the number of frequency points allows the use of higher carrier frequency signals, thereby improving the system's measurement accuracy and range. However, as the number of frequency points increases, the peak-to-average power ratio (PAPR) of the signal also increases. The relationship between the number of frequencies and PAPR is shown in Fig. 2(b). To ensure that electro-optical conversion and RF amplifiers operate within their linear regions, it is necessary to reduce the signal power for each frequency point. This reduction in power leads to decreased phase accuracy for each frequency point, which impacts OTD measurement accuracy and the ability to perform ambiguity-free measurements. For a larger number of frequency points, additional algorithms, such as partial transmit sequence (PTS), are needed to suppress high PAPR. In the following experimental section, we design a scheme that includes an optical path reference to mitigate the third-order intermodulation distortion caused by the PAPR of the MFC signals in the measurement system.

In practical terms, each microwave source must be precisely locked, which means that increasing the number of frequency points adds both complexity and cost to the system. Additionally, a larger number of frequency points raises the computational complexity of the back-end process. Fewer frequency points are generally more advantageous for implementing a simple, low-cost measurement system. In cases where the SNR of the link under test is limited, it may be necessary to increase the number of frequency points to relax the required phase accuracy. If the measurement system exhibits high linearity, it might also be beneficial to increase the frequency points to improve the system's robustness in terms of ambiguity-free measurement capabilities.

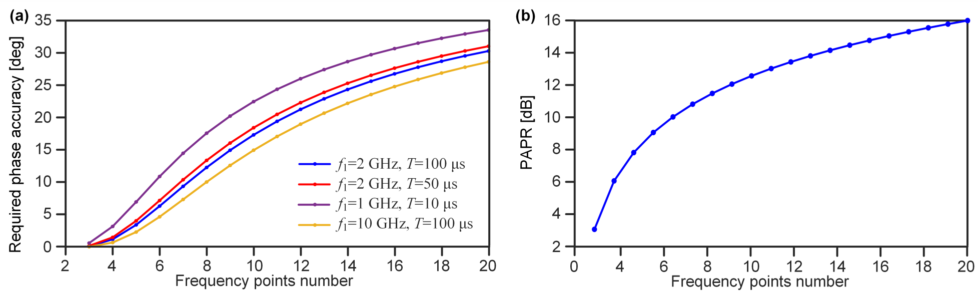

Fig. 2. Relationships between the number of frequency points and (a) the required phase accuracy, and (b) the peak-to-average power ratio (PAPR).

3. Experiment and discussion

We demonstrate two single-shot OTD measurement system implementations based on a nonlinear interval MFC. The first one employs an electrical path reference, as shown in Fig. 3(a). The continuous-wave light generated from a laser source (TeraXion, PS-TNL) is sent into an intensity modulator (IXBlue, MX-LN-40). The modulator is driven by a coherent RF source comprising four synchronized microwave sources $f_1 \sim f_4$ (Rohde Schwarz, SMB100A) with frequencies of 2, 2.015, 2.0302, and 2.045403 GHz. Based on the proposed phase unwrapping algorithm, the first step is calculating the phase difference with an interval of 3 kHz. The integer ambiguity of 200 kHz, 15 MHz, and 2 GHz can be calculated step-by-step using the magnification factors $\Delta f_2/\Delta f_1$, $\Delta f_3/\Delta f_2$, and $\Delta f_4/\Delta f_3$, which are 66.7, 75, and 133.3 respectively. To prevent errors in resolving ambiguity, the phase detector must have an accuracy of ±0.6701 deg. After passing through the optical path, the optical signal is detected by a 10-GHz photodetector (CONQUER, KG-PD-10G). An oscilloscope (Keysight, 86100C Infiniium DCA) with a sampling rate of 10 GSa/s is applied as a dual-port ADC to acquire the probe and reference signals simultaneously. The sampling time length is set as 10 μs.

3.1. Process of phase detection and phase unwrapping

Since the frequencies in the MFC are known and sparse, we can efficiently calculate the signal's phase by directly multiplying the detected signal with a series of specific fast Fourier Transform (FFT) kernels. This method reduces the number of floating-point operations from $\frac{5}{2}N\log_2\frac{N}{2}$ to $16N$, offering a substantial decrease in computational complexity. With a data volume of 10 GSa/s×10 μs=10^5 Sa, our proposed measurement method achieves at least a fourfold reduction in computational overhead. The total number of floating-point operations per second is (16×10^5) FLOPs×2 Channels×100 kHz=0.32 TFLOPs, well within the processing capabilities of commercial FPGAs such as the Xilinx Virtex UltraScale+ and Intel Stratix 10. For further enhancements, additional sparse FFT algorithms can be implemented to achieve even greater calculation speeds.

The proposed phase unwrapping algorithm is validated by measuring an optical fiber of 20.18 km. From the condition $\tau \le 1/(2\times\Delta f_1)$, the system can achieve a measurement range of over 166.67 μs = 1/(2×3 kHz). Before the measurement, a calibration process is performed to remove the system length. The detected phases of the aforementioned RF signals are -71.220 deg, 111.917 deg, -130.203 deg, and -122.457 deg. By performing the phase unwrapping algorithm, the calculated results of the integer ambiguity N(200 kHz), N(15 MHz), and N(2 GHz) are 20, 1513, and 201799, respectively. Finally, according to Eq. (3), the OTD under test is calculated as 100.89959892 μs.

In the proposed OTD measurement system, the choice of frequency interval is determined by

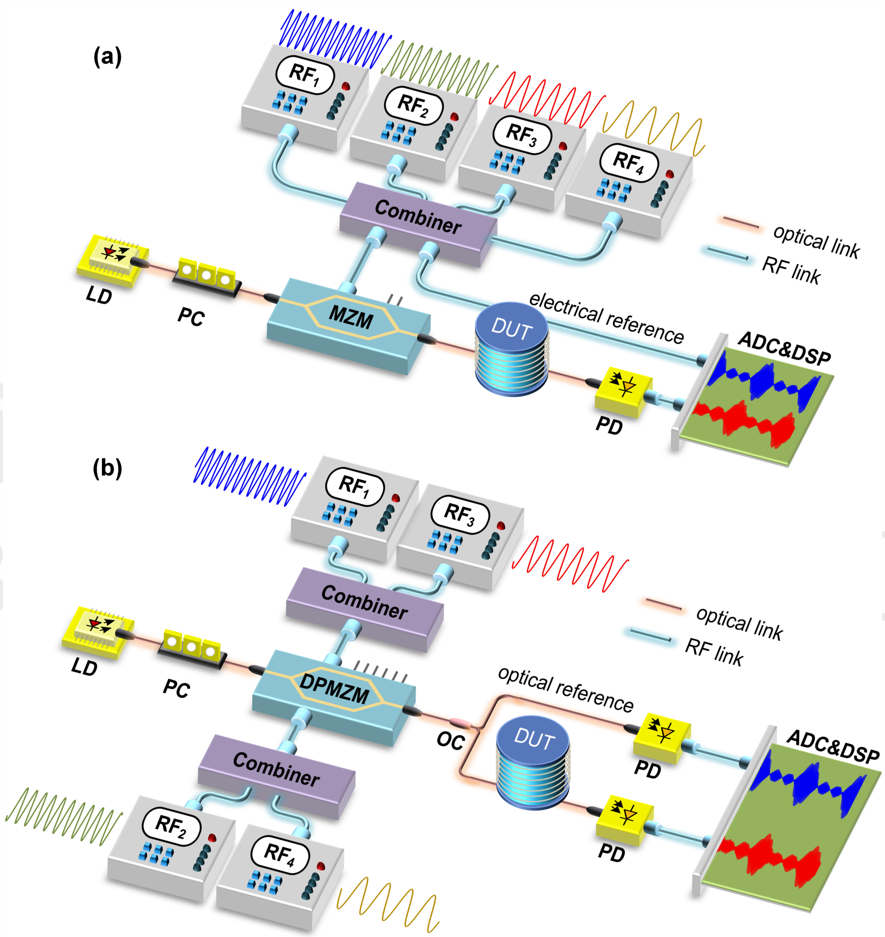

Fig. 3. Two implementations of the single-shot OTD measurement system. (a) OTD measurement with electrical path reference. (b) OTD measurement with optical path reference. LD, laser diode; MZM, Mach-Zehnder modulator; DPMZM, dual-parallel Mach-Zehnder modulator; OC, optical coupler; RF, radio-frequency; PD, photodetector; ADC, analog-to-digital converter; DSP, digital signal processor.

the phase detection accuracy. In this section, we present a model for phase error under digital phase detection and experimentally validate that it meets the requirements for phase unwrapping. The phase error, denoted as σ_θ, is typically attributable to three primary factors. We represent the equation as following:

$$\sigma_\theta = \sqrt{\sigma_{SNR}^2 + \sigma_f^2 + \sigma_D^2}, \tag{13}$$

The initial term σ_{SNR}^2, is influenced by the SNR and can be expressed as $\sigma_{SNR}^2 \propto 1/(f_s \cdot T_s \cdot SNR)$, where f_s represents the sampling rate, T_s the sampling time, and SNR the signal-to-noise ratio itself. The subsequent term, $\sigma_f = 2\pi \cdot \Delta f \cdot \tau$, represents the frequency stability of the microwave signal, with Δf indicating the frequency deviation and τ the measured delay. Here, only the short-term stability of the microwave source is considered, as its long-term stability can be maintained by locking it to a commercial atomic clock, which typically achieves 10^{-12}. The phase detection error introduced by long-term frequency drift is negligible compared to the impact of the SNR. The final term, $\sigma_D = \beta_3 \cdot (2\pi f)^3 \cdot L/6$, accounts for waveguide dispersion, where β_3 denotes the third-order dispersion coefficient, f the microwave frequency, and L the length of the waveguide. Using SMF-28 optical fiber as an example, which has a third-order dispersion coefficient of approximately 0.116 $ps^3/rad^2/km$ at 1550 nm, even a 100 km single-mode optical fiber introduces only a negligible phase error of 2.2×10^{-4} deg.

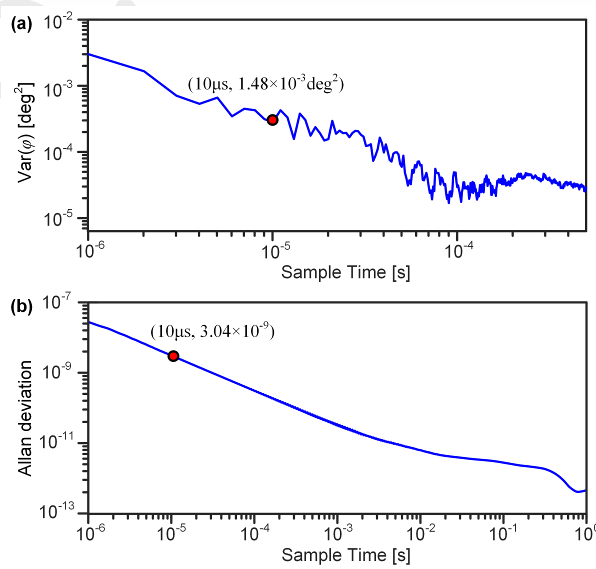

Fig. 4. The relationship between sampling time and two key variables: (a) phase variance and (b) short-term frequency stability.

Two experiments were conducted to assess the impact of SNR and frequency stability, influenced by the length of the sampling time. The first experiment measures phase variance over sampling time ranging from 1 to 500 μs in a 5 ms data. The results, shown in Fig. 4(a), indicate that with 10 μs sampling time, the phase jitter induced by SNR is 0.03 deg (1.48×10^{-3} deg^2). In the second experiment, a phase noise analyzer (Rohde Schwarz, FSWP) is used to evaluate the phase noise of the MFC. The tools allow the calculation of short-term frequency stability through the integral of phase noise. Fig. 4(b) shows an Allan deviation of 3.04×10^{-9} for a 10 μs sampling period. According to the formula, the phase jitter induced by the frequency drift in a 20 km optical fiber is calculated to be less than 360 deg $\times$ $3.04\times10^{-9}\times$2 GHz×100 μs=0.22

deg. In the proposed phase unwrapping algorithm, the required phase error must remain below ±0.67 deg. Therefore, the error introduced by the short-term stability of the microwave source will not cause the phase unwrapping algorithm to fail in the experiment. Overall, the proposed OTD measurement system theoretically satisfies the requirements for an absolute 20 km optical fiber with sub-picosecond accuracy and a 100 kHz refresh rate.

3.2. Third-order intermodulation distortion and its suppression method

Although the discrete frequency sampling method avoids the frequency overlap problem, MFC with a high PAPR can lead to nonlinear distortion in both the electrical and optical links. Specifically, if the frequency interval between the MFC and the intermodulation frequency component is narrower than the bandwidth of the IF filter, additional phase error will be introduced in the phase detection.

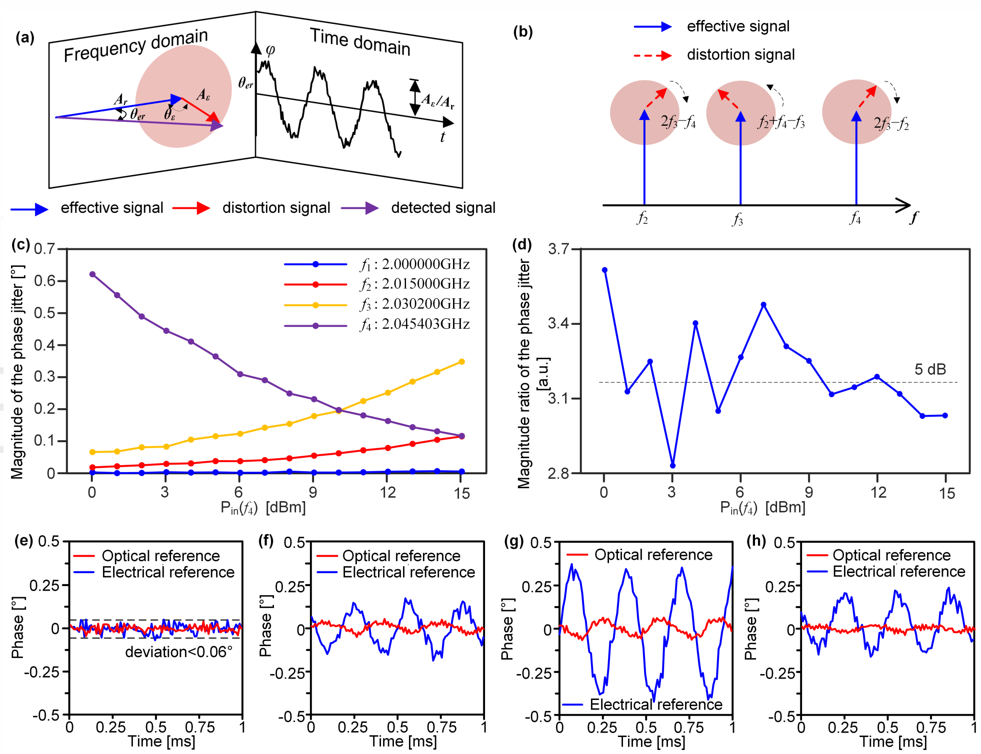

Fig. 5. (a) Modeling of the third-order intermodulation distortion in the frequency and time domains. (b) The effect of third-order intermodulation distortion of the received signal. (c) The magnitude of the 3 kHz periodic phase jitter induced by the third-order intermodulation distortion interference. The power of frequency points f_1 and f_2 are kept at 15 dBm, f_3 is kept at 10 dBm, while the frequency point f_4 varies from 0 dBm to 15 dBm. (d) The magnitude ratio of the periodic phase jitter relationship between f_2 and f_3. (e)~(f): Phase detection results of $f_1 \sim f_4$. within 1 ms when the modulated signal power of $f_1 \sim f_4$ is 15, 15, 10, 15 dBm.

To assess the impact of intermodulation distortion, we assume that the amplitudes of the effective signal and the distortion signal are denoted as A_r and A_ϵ, respectively, and that the phase difference between the two is θ_ϵ. The phasor diagram of the detected signal, effective signal, and distortion signal is presented in Fig. 5(a). Applying the law of sines, we can obtain the equation:

$$\frac{A_\epsilon}{A_r} = \frac{\sin(\theta_{\text{er}})}{\sin(\theta_{\text{er}} - \theta_\epsilon)}, \tag{14}$$

where θ_{er} is the phase error induced by the distortion signal. Considering that the distortion signal has a relatively low amplitude compared to the effective signal, i.e., $A_\epsilon / A_r << 1$. Therefore, the phase error (θ_{er}) is approximate to the following expression:

$$\begin{aligned}\theta_{\text{er}} &= \arctan(\tan(\theta_{\text{er}})) \\ &= \arctan\Big(\frac{\sin(\theta_\epsilon)}{A_r/A_\epsilon - \cos(\theta_\epsilon)}\Big) \\ &\approx \frac{A_\epsilon}{A_r}\sin(\theta_\epsilon) = \sqrt{\frac{P_\epsilon}{P_r}}\sin(\theta_\epsilon).\end{aligned} \tag{15}$$

According to Eq. (15), the phase error is determined by the amplitude ratio A_ϵ / A_r and the phase difference θ_ϵ. In the experiment, the frequency components f_2 (distortion frequency is $2f_3 - f_4 = f_2 - 3$ kHz), f_3 (distortion frequency is $f_2 + f_4 - f_3 = f_3 + 3$ kHz), and f_4 (distortion frequency is $2f_3 - f_2 = f_4 - 3$ kHz) would be affected by the distortion signal, as illustrated in the schematic spectrum in Fig. 5(b). If the bandwidth IF filter exceeds 3 kHz, the phase difference θ_ϵ will introduce a periodic time-varying error with a period of 333 µs≈ 1/(3 kHz). To observe this phenomenon, we set the power of the frequency points f_1 and f_2 to 15 dBm, f_3 to 10 dBm, while varying the power of f_4 from 0 to 15 dBm. Fig. 5(c) shows the measurement results of the magnitude of the 3-kHz frequency component of the phase changes during a period of 1 ms with a sampling time of 10 µs. As the power of f_4 increases, the frequency points f_2 and f_3 are increasingly affected by the intermodulation distortion. The magnitude ratio of the periodic jitter between f_2 and f_3 is given in Fig. 5(d). In theory, the magnitude ratio of the phase jitter should equal the power ratio P_2/P_3, i.e., 5 dB. On the contrary, the effect of the intermodulation distortion on the frequency point f_4 decreases because the amplitude ratio A_ϵ / A_r decreases. The frequency point f_1 is not impacted by the intermodulation distortion, which fits well with the theoretical model.

In practice, the RF power should be set to a high level to ensure accurate measurements of a large insertion link. However, this approach inevitably results in a high PAPR and significant intermodulation distortion in the MFC-based OTD measurement system. To address this issue, we propose a novel single-shot OTD measurement system based on optical path reference. As shown in Fig. 3(b), we replace the intensity modulator with a dual-parallel Mach-Zehnder modulator (DPMZM, Fujitsu, FTM7961). RF_1 and RF_3 are combined and injected into the upper branch of the DPMZM, while RF_2 and RF_4 are combined and injected into the lower branch. According to the above theory analysis, the intermodulation distortion frequencies include f_3. To suppress the intermodulation distortion, the OTD measurement system based on the optical path reference separates the frequency f_3 from f_1 and f_2 during the modulation process. The probe and the reference are sent to two photodetectors in the receiver.

Fig. 5(e)~(h) shows the phase detection results of four frequencies within 1 ms under large signal modulation. The injected power of the MFC is 15 dBm. As can be seen, the optical reference implementation provides better suppression of the intermodulation distortion. The suppression ratios of the 3-kHz periodic phase error at the frequency points f_2, f_3, and f_4 are 5.65 dB, 6.84 dB, and 8.41 dB, respectively. It should be emphasized that only f_1 directly affects the measurement accuracy, while the other frequencies are used for phase unwrapping. Therefore, to ensure the accuracy of phase unwrapping, the phase fluctuation of these frequencies needs to comply with Eq. (10).

3.3. System stability and measurement accuracy

To assess the stability of the proposed OTD measurement system, we experimented with no devices connected to the measurement branch. As depicted in Fig. 6(a), the OTD remained within a fluctuation range below ±0.1 ps for over 20 minutes. This indicates that in a relatively stable indoor environment, the measurement system's long-term stability is better than ±0.1 ps. In most practical applications, the measurement system can be placed indoors where the environment is relatively stable, with the test link connected via optical fiber. This approach helps mitigate the impact of environmental changes on the stability of the system.

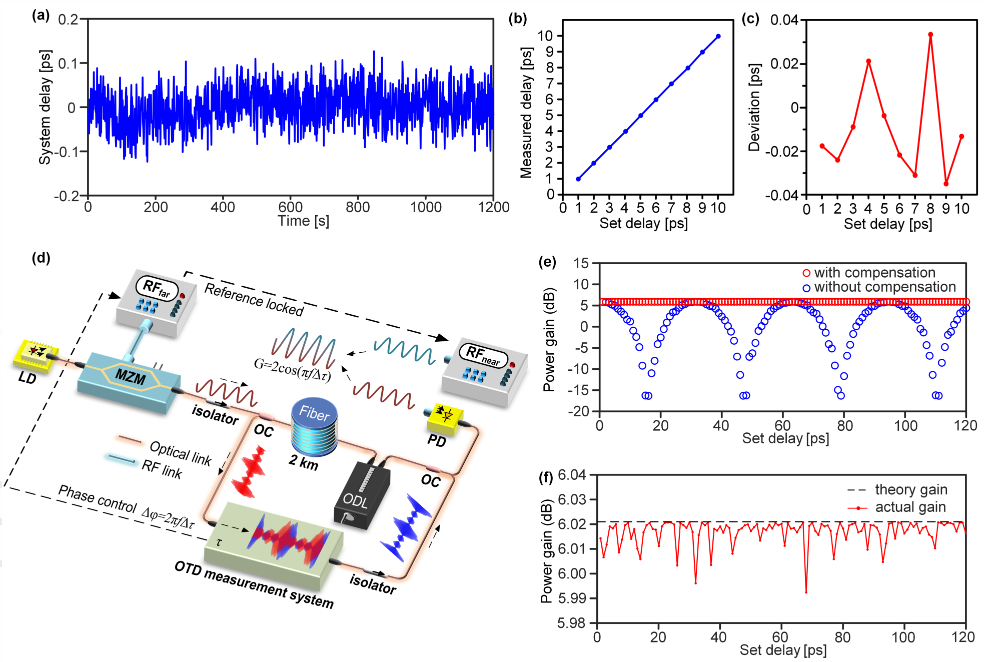

Fig. 6. (a) Experimental results of the system stability over 20 minutes; (b) The measured delay of the motorized delay line from 10 ps to 1 ps; (c) The deviation of the measured delay line. (d) Schematic diagram of distributed coherent aperture experiment with OTD measurement and compensation. G is the gain of coherent aperture synthesis. (e) Power gain of the coherent synthetic with different OTD differences. (f) Detailed power gain of the coherent synthetic with compensated OTD.

Furthermore, we conducted another experiment to evaluate the measurement accuracy of the system, utilizing a motorized variable optical delay line (General Photonics MDL-002) as a DUT. The optical delay line has a resolution of less than 1 fs and an accuracy level of ±10 fs. As shown in Fig. 6(b), the delay line was set to sweep from 1 ps to 10 ps, and the measured OTD was well-matched with the set value. According to Fig. 6(c), the measurement deviation from the set value is within ±0.04 ps.

We have also implemented a distributed coherent aperture synthesis experiment based on the proposed OTD measurement. Generally, the theoretical gain of the coherent synthesis can be expressed by the following formula:

$$
\begin{aligned}
G &= 20 \cdot \log_{10}\left(\left|\frac{A_1 + A_2 \cdot \exp j(2\pi f \Delta\tau)}{A_1}\right|\right) \\
&= 10 \cdot \log_{10}\left(1 + \frac{A_2^2}{A_1^2} + 2\frac{A_2}{A_1}\cos(2\pi f \Delta\tau)\right),
\end{aligned}
\tag{16}
$$

where A_1 and A_2 are the amplitudes of the signals to be synthesized, f is the frequency of the signals, and $\Delta\tau$ is the delay difference between the two signals. It can be seen that both the delay difference and amplitude ratio between the two signals affect the coherent synthesis gain.

The proof-of-concept experiment structure is shown in Fig. 6(d). Two RF sources, RF_{far} and RF_{near}, locked to the same reference local oscillator, generate a single-frequency microwave signal with a frequency of 31.8 GHz. RF_{far} is transmitted through a 2-km long radio-over-fiber (RoF) link. The proposed single-shot measurement system conducts a real-time measurement of the transmission link. A dual-port ADC then acquires the two signals with an 80 Gbit/s sampling rate, and their amplitude is normalized in the digital domain. A digital synthesis is subsequently performed to combine the two signals, with the initial phase of RF_{far} adjusted according to the measured OTD (i.e., $\varphi_{\text{initial}} = 2\pi f \Delta\tau$) to maximize the coherent synthetic gain. The phase-controlling resolution is 0.001 deg. The optical delay line is set to sweep from 1 to 120 ps. The power gain of the coherent synthetic is shown in Fig. 6(e). If the distributed coherent aperture system does not compensate for the delay variation, a few picoseconds variations will lead to a power attenuation of over 20 dB. Fig. 6(f) provides a detailed result of the delay compensation. According to Eq. (16), the theoretical maximum power gain of two signals is 6.0206 dB (i.e., $20\log_{10}2$). The average measured power gain is 6.0168 dB. If we assume that the two signals are maintained at the same amplitude, this power gain corresponds to a delay error of 0.3 ps. The delay compensation performs an effective role in the distributed coherent aperture synthesis.

3.4. Single-shot measurement

A fast-switched OTD link is also constructed to verify the speed and range performance of the single-shot measurement system. The incoming optical signal is injected into a 1×2 magneto-optical optical switch (Primanex, MagLight 1×2), which has a switching time of approximately 100 µs. A square wave signal with a period of 1 ms and a duty ratio of 50% is applied as the driven signal to switch the channels at a fast speed. Two fibers with 10 km and 20 km are connected to the two output ports of the switch. The measurement results are presented in Fig. 7(a). The length of the sampling time is set to 10 µs. The OTDs of the different segments are 50.2824203 µs and 100.8995992 µs without any ambiguous values. During the switching time, the measured OTD is not valid because the optical signal is cut off. Here, we achieve a standard deviation (STD) below 0.2 ps when the absolute OTD exceeds 100 µs, corresponding to a relative uncertainty of 2×10^{-9}. We also compare our method with other state-of-the-art technologies, which is given in Fig. 7(b). To the best of our knowledge, this is the first time that a measurement uncertainty of 10^{-9} level has been disclosed with a single sampling time of 10 µs. Overall, the proposed system achieves a measurement range of over 100 µs, a precision of sub-picosecond, and a response speed of 100 kHz. The general OTD measurement method, when no prior knowledge is available, employs a maximum likelihood estimation approach, maximizing the measurement SNR through matched filtering techniques. Analog-domain matched filtering has almost no computational overhead during the measurement process but makes it difficult to adjust and optimize system performance and parameter specifications [31, 34]. Digital-domain matched filtering, on the other hand, typically involves operations such as convolution [35], FFT [20, 23, 29, 36, 37], Hilbert transform [32], or in-phase and quadrature (I/Q) demodulation [26], with computational complexities ranging from $O(N^2)$, $O(N\text{logN})$, to $O(N)$, where N represents the number of sampling points. Our method requires extracting the phase of four known frequency components,

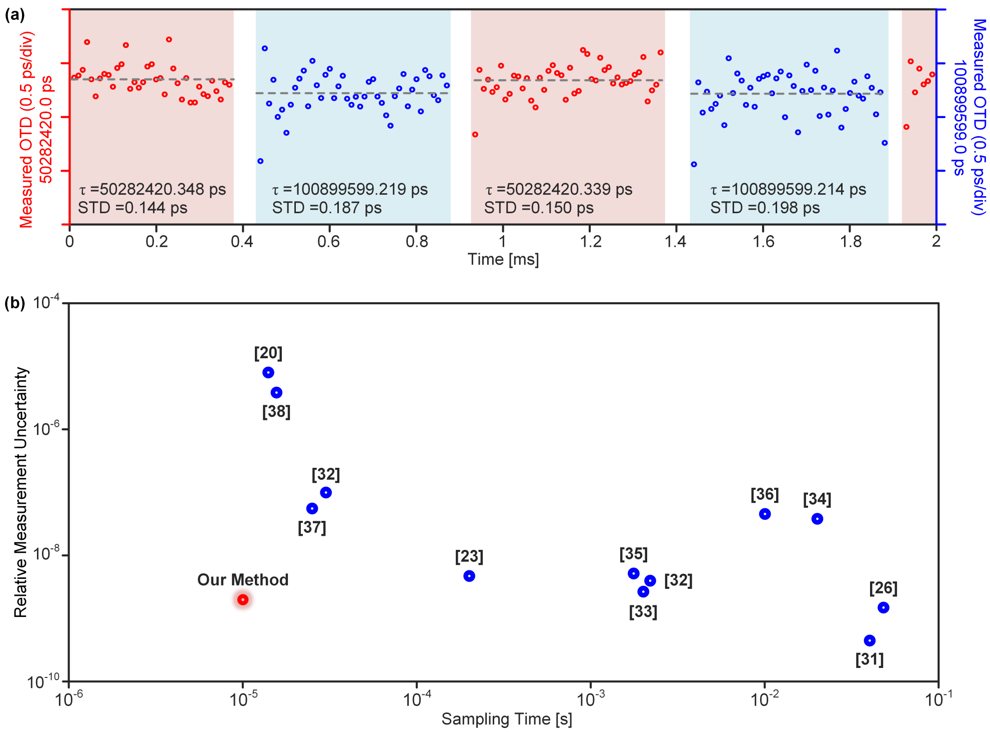

Fig. 7. (a) Verification experiment of the measurement speed and measurement range. Blue dot: 20-km fiber link. Red dot: 10-km fiber link. (b) Comparison with other optical delay measurement and ranging methods [20, 23, 26, 29, 31–38].

resulting in a computational complexity of $O(N)$. Compared to other types of digital-domain matched filtering methods, the proposed single-shot method has relatively low computational complexity. By adding analog down-conversion modules in hardware, it is possible to further reduce the number of sampling points and computational overhead, thereby decreasing the dependence on high-performance receivers.

It should be noted that the achieved measurement capability here is highly required in many systems. For instance, in distributed MIMO communication systems, the delay of each channel should be synchronized with high accuracy. However, there is very limited synchronization time allowed between the central station and the base station (usually with a large range) to ensure uninterrupted communication. Additionally, it should be emphasized that the proposed MFC-based OTD measurement method relies on the linear phase assumption of the transmission link. This reliance enables the use of discrete frequency sampling to characterize OTD without needing a measurement signal covering a large frequency band, unlike previous methods. However, in scenarios where the optical link under test contains nonlinear elements, such as micro-rings or fiber Bragg gratings, a more complex model than the linear phase assumption is necessary for accurate and real-time OTD characterization.

4. Conclusion

In conclusion, we propose a single-shot, high-accuracy, and long-range OTD measurement system tailored for emerging distributed systems. Utilizing a phase-locked nonlinear interval MFC as the probe signal, the proposed system overcomes the traditional limitations of phase-derived ranging technology. This is achieved through innovative discrete frequency sampling and a novel phase unwrapping method, enabling a 100 kHz refresh rate for continuous measurement. Furthermore, we introduce a new architecture incorporating an optical path reference to circumvent third-order intermodulation distortion. By suppressing the periodic phase error by 5.65 dB, the measurement accuracy is further improved. Our experimental results demonstrate a measurement accuracy of 0.3 ps and a relative uncertainty of 2×10^{-9}. Overall, we believe the proposed OTD measurement system provides a robust and precise tool that effectively meets the critical demands of distributed communication and radar systems.

Funding. National Natural Science Foundation of China (Nos.62271249 and 62075095), Fundamental Research Funds for the Central Universities, and Funding for Outstanding Doctoral Dissertation in NUAA (BCXJ24-09).

Acknowledgments. This work was funded by the National Natural Science Foundation of China (Nos.62271249 and 62075095), Fundamental Research Funds for the Central Universities, and Funding for Outstanding Doctoral Dissertation in NUAA (BCXJ24-09).

Disclosures. The authors declare no conflicts of interest.

Data Availability Statement. The data underlying the results presented in this paper are not publicly available at this time but may be obtained from the authors upon reasonable request.

References

1. J. T. Mok and B. J. Eggleton, "Expect more delays," Nature **433**, 811–812 (2005).
2. L. Zhuang, M. Hoekman, W. Beeker, *et al.*, "Novel low-loss waveguide delay lines using vernier ring resonators for on-chip multi-λ microwave photonic signal processors," Laser & photonics reviews **7**, 994–1002 (2013).
3. T. Chen, Z. Dang, Z. Deng, *et al.*, "Large-scale optical switches by thermo-optic waveguide lens," PhotoniX **5**, 14 (2024).
4. F. Kaneda and P. G. Kwiat, "High-efficiency single-photon generation via large-scale active time multiplexing," Sci. Adv. **5**, eaaw8586 (2019).
5. W. Ng, A. A. Walston, G. L. Tangonan, *et al.*, "The first demonstration of an optically steered microwave phased array antenna using true-time-delay," J. Light. technology **9**, 1124–1131 (1991).
6. T. Nagayama, S. Akiba, T. Tomura, and J. Hirokawa, "Photonics-based millimeter-wave band remote beamforming of array-antenna integrated with photodiode using variable optical delay line and attenuator," J. Light. Technol. **36**, 4416–4422 (2018).
7. X. Xiao, S. Li, S. Peng, *et al.*, "Photonics-based wideband distributed coherent aperture radar system," Opt. Express **26**, 33783–33796 (2018).
8. J. Wang, H. Shen, L. Fan, *et al.*, "Reconfigurable radio-frequency arbitrary waveforms synthesized in a silicon photonic chip," Nat. Commun. **6**, 5957 (2015).
9. I. C. Sezgin, M. Dahlgren, T. Eriksson, *et al.*, "A low-complexity distributed-mimo testbed based on high-speed sigma–delta-over-fiber," IEEE Trans. on Microw. Theory Tech. **67**, 2861–2872 (2019).
10. K. Zhang, B. Zhu, Z. Zhang, and H. Wang, "Tracking system for fast moving nodes in optical mobile communication and the design rules," IEEE Trans. on Wirel. Commun. **20**, 2716–2728 (2020).
11. A. Weiss and E. Weinstein, "Fundamental limitations in passive time delay estimation–part i: Narrow-band systems," IEEE Trans. on Acoust. Speech, Signal Process. **31**, 472–486 (1983).
12. E. Weinstein and A. Weiss, "Fundamental limitations in passive time-delay estimation–part ii: Wide-band systems," IEEE Trans. on Acoust. Speech, Signal Process. **32**, 1064–1078 (1984).
13. Y. Lu, T. Zhu, L. Chen, and X. Bao, "Distributed vibration sensor based on coherent detection of phase-otdr," J. Light. Technol. **28**, 3243–3249 (2010).
14. D. L. Philen, I. A. White, J. F. Kuhl, and S. C. Mettler, "Single-mode fiber otdr: Experiment and theory," IEEE Trans. on Microw. Theory Tech. **30**, 1487–1496 (1982).
15. W. Eickhoff and R. Ulrich, "Optical frequency domain reflectometry in single-mode fiber," Appl. Phys. Lett. **39**, 693–695 (1981).
16. Z. Ding, X. S. Yao, T. Liu, *et al.*, "Compensation of laser frequency tuning nonlinearity of a long range ofdr using deskew filter," Opt. Express **21**, 3826–3834 (2013).
17. F. Ito, X. Fan, and Y. Koshikiya, "Long-range coherent ofdr with light source phase noise compensation," J. Light. Technol. **30**, 1015–1024 (2011).
18. J. Dong, B. Wang, C. Gao, *et al.*, "Highly accurate fiber transfer delay measurement with large dynamic range," Opt. Express **24**, 1368–1375 (2016).
19. K. Yun, J. Li, G. Zhang, *et al.*, "Simple and highly accurate technique for time delay measurement in optical fibers by free-running laser configuration," Opt. Lett. **33**, 1732–1734 (2008).
20. P. Trocha, M. Karpov, D. Ganin, *et al.*, "Ultrafast optical ranging using microresonator soliton frequency combs," Science **359**, 887–891 (2018).

21. E. D. Caldwell, L. C. Sinclair, N. R. Newbury, and J.-D. Deschenes, “The time-programmable frequency comb and its use in quantum-limited ranging,” Nature **610**, 667–673 (2022).
22. N. Lippok and B. J. Vakoc, “Resolving absolute depth in circular-ranging optical coherence tomography by using a degenerate frequency comb,” Opt. Lett. **45**, 371–374 (2020).
23. J. Wang, Z. Lu, W. Wang, *et al.*, “Long-distance ranging with high precision using a soliton microcomb,” Photonics Res. **8**, 1964–1972 (2020).
24. M.-G. Suh and K. J. Vahala, “Soliton microcomb range measurement,” Science **359**, 884–887 (2018).
25. Z. Zhu and G. Wu, “Dual-comb ranging,” Engineering **4**, 772–778 (2018).
26. S. Li, T. Qing, J. Fu, *et al.*, “High-accuracy and fast measurement of optical transfer delay,” IEEE Trans. on Instrum. Meas. **70**, 1–4 (2020).
27. L. Wang, X. Liu, X. Chen, *et al.*, “Speed-enhanced optical fiber transfer delay measurement based on digital phase detecting,” in *2021 Asia Communications and Photonics Conference (ACP),* (IEEE, 2021), pp. 1–3.
28. Q. Sun, C. Liu, J. Yang, *et al.*, “Phase-derived ranging based fiber transfer delay measurement using a composite signal for distributed radars with fiber networks,” Photonics **10**, 421 (2023).
29. B. Qiu, Y. Zhang, X. Sun, *et al.*, “Laser ranging with micrometer precision and khz rate via joint frequency-phase measurement,” IEEE Photonics Technol. Lett. **34**, 1214–1217 (2022).
30. L. Cohen, *Time-frequency analysis*, vol. 778 (Prentice Hall PTR New Jersey, 1995).
31. T. Xie, J. Wang, Z. Wang, *et al.*, “Long-range, high-precision, and high-speed absolute distance measurement based on alternately oscillating optoelectronic oscillators,” Opt. Express **27**, 21635–21645 (2019).
32. Y. Zhang, Z. Zeng, L. Zhang, *et al.*, “Ultrafast and high-precision time delay measurement based on complementary frequency-swept light and frequency-shifted dechirping,” J. Light. Technol. **42**, 1927–1933 (2023).
33. Y.-S. Jang, J. Park, and J. Jin, “Sub-100-nm precision distance measurement by means of all-fiber photonic microwave mixing,” Opt. Express **29**, 12229–12239 (2021).
34. Y. Na, C.-G. Jeon, C. Ahn, *et al.*, “Ultrafast, sub-nanometre-precision and multifunctional time-of-flight detection,” Nat. Photonics **14**, 355–360 (2020).
35. Q. Niu, J. Zheng, X. Cheng, *et al.*, “Arbitrary distance measurement without dead zone by chirped pulse spectrally interferometry using a femtosecond optical frequency comb,” Opt. Express **30**, 35029–35040 (2022).
36. J. Zheng, L. Jia, Y. Zhai, *et al.*, “High-precision silicon-integrated frequency-modulated continuous wave lidar calibrated using a microresonator,” ACS Photonics **9**, 2783–2791 (2022).
37. Y.-S. Jang, S. Eom, J. Park, and J. Jin, “Programmable spectral shaping for nanometric precision of frequency comb mode-resolved spectral interferometric ranging,” Opt. & Laser Technol. **170**, 110324 (2024).
38. C. Zhang, Z. Zhang, Y. Tian, *et al.*, “Comprehensive ranging disambiguation for amplitude-modulated continuous-wave laser scanner with focusing optics,” IEEE Trans. on Instrum. Meas. **70**, 1–11 (2020).